Electronic Supplementary Material (ESI) for Physical Chemistry Chemical Physics.
This journal is © the Owner Societies 2022

Electronic Supplementary Information for: "Interaction between two polyelectrolytes in monovalent aqueous salt solutions"

Xiang Yang,*[a] Alberto Scacchi,[abc] Hossein Vahid,[abc] Maria Sammalkorpi,[bcd] and Tapio Ala-Nissila[aef]

1 Root-mean-square error analysis

We optimize the parameters σ^{B} and a^{*}_{SPB} by minimizing the root-mean-square error (RMSE) between the Cl^{-} density profile obtained from the different models. The definition of RMSE between two density profiles $\rho_1(r)$ and $\rho_2(r)$ is defined as:

$$\mathrm{RMSE} = \frac{1}{\sqrt{N}}\sqrt{\sum_{k=1}^{N} \mid \rho_1(r_k) - \rho_2(r_k) \mid^2}, \tag{S1}$$

where N is the number of sampling points.

Specifically, in order to obtain the effective diameter of the PE in the CG model, σ^{B}, ρ_1 is replaced by ρ^{Cl} from all-atom MD simulations, whereas ρ_2 by $\rho^{\mathrm{Cl}}_{\mathrm{CG}}$, obtained from the CG model, which depends on σ^{B}. The values of the optimized diameter σ^{B} for different salt concentrations are shown in Table. S1. We choose the average over the four salt concentrations, i.e. $\sigma^{\mathrm{B}} = 0.54$ nm.

On the other hand, in the case of SPB theory, ρ_2 is replaced by $\rho^{\mathrm{Cl}}_{\mathrm{SPB}}$, which depends on a_{SPB}. The optimal values from fitting a^{*}_{SPB} at different salt concentrations are shown in Table S1. Also in this case we choose the average over the different salt concentrations, i.e. $a^{*}_{\mathrm{SPB}} = 0.44$ nm, used throughout the work (also for the SLPB theory).

Table S1 The optimal values of σ^{B}, σ^{BCl} obtained for the CG model and a^{*}_{SPB} for the SPB theory in different salt concentrations.

ρ_0 [M]	0.13	0.26	0.52	1.0
σ^{B} [nm]	0.54	0.54	0.52	0.54
σ^{BCl} [nm]	0.46	0.46	0.45	0.46
a^{*}_{SPB} [nm]	0.50	0.45	0.43	0.39

2 Soft potential enhanced linear Poisson-Boltzmann theory

When $\beta e \phi(r) \ll 1$, which corresponds to small electrostatic potentials, we can linearize the full PB equation. This linear approximation is commonly referred to as the Debye-Hückel approximation.

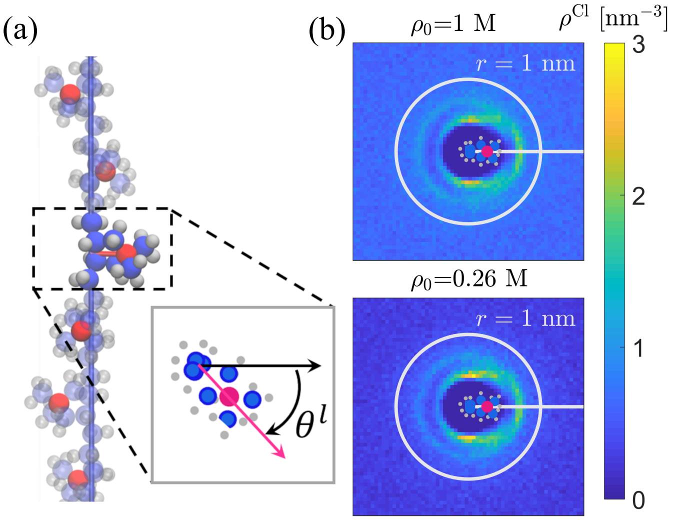

Fig. S1 (a) The l^{th} monomer in the PDADMA is shown in the zoomed inset. The atomistic structure is projected onto the (r,θ) plane and the orientation of N^{+} is recorded as θ^{l}; the N^{+}, C and H atoms are colored in red, blue, and gray, respectively. From (a) to (b), the orientation of a N^{+} atom in the l^{th} monomer and the ion number density $\rho^{\mathrm{Cl},l}$ around it are rotated by $-\theta^{l}$. Then $\rho^{\mathrm{Cl},l}$ are averaged over l to get ρ^{Cl} in panel (b) for different salt concentrations. In the center of each density map we schematically show the atomistic structure of one monomer.

Equation (3) in the main text then becomes

$$\nabla^2 \phi_{\mathrm{LPB}}(r) = \kappa^2 \phi_{\mathrm{LPB}}(r), \tag{S2}$$

where $1/\kappa$ is the Debye or screening length[1]. The analytic solution of Eq. (S2) for $r > a$ is[2]

$$\phi_{\mathrm{LPB}}(r) = \frac{\lambda}{2\pi a \kappa \varepsilon}\frac{K_0(\kappa r)}{K_1(\kappa a)}, \tag{S3}$$

where K_0 and K_1 are modified Bessel functions of order zero and one, correspondingly. The soft-potential enhancement can be used for both the full and linearized PB theories. Finally, for the two-PE case, the corresponding force from the linear theory f_{SLPB} and the potential of mean force (PMF) are obtained by numerically solving Eq. (S2) similarly to the full PB equation, with the boundary conditions at the surface of the two disks with radii $a = a_{\mathrm{SLPB}}$ (cf. Fig. 1(g) in the main text) $\nabla\phi \cdot \hat{n}|_{x^2+y^2=a^2} = \lambda/2\pi a \varepsilon$ and $\nabla\phi \cdot \hat{n}|_{(x-d)^2+y^2=a^2} = \lambda/2\pi a \varepsilon$.

3 The atomic structure of PDADMA

Our atomistic PDADMA MD model consists of 10 monomers and the polymer axis is set along the z direction. Each monomer cor-

---

[a] *Department of Applied Physics, Aalto University, P.O. Box 11000, FI-00076 Aalto, Finland*
[b] *Department of Chemistry and Materials Science, Aalto University, P.O. Box 16100, FI-00076 Aalto, Finland*
[c] *Academy of Finland Center of Excellence in Life-Inspired Hybrid Materials (LIBER), Aalto University, P.O. Box 16100, FI-00076 Aalto, Finland*
[d] *Department of Bioproducs and Biosystems, Aalto University, P.O. Box 16100, FI-00076 Aalto, Finland*
[e] *QTF Center of Excellence, Department of Applied Physics, Aalto University, P.O. Box 11000, FI-00076 Aalto, Finland*
[f] *Interdisciplinary Center for Mathematical Modelling and Department of Mathematical Sciences, Loughborough University, Loughborough, Leicestershire LE11 3TU, UK*

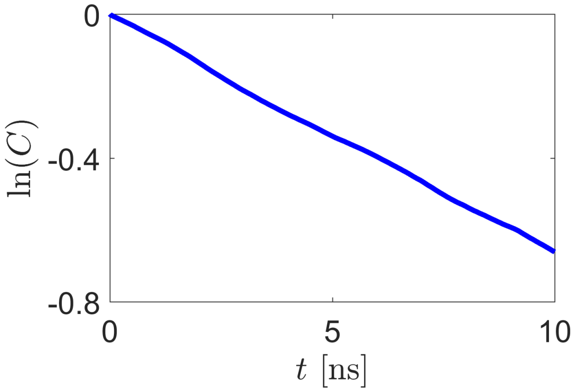

Fig. S2 The orientational self-correlation function of a single PDADMA as a function of time t on a semilogarithmic scale. The correlation time $t_c = 15$ ns corresponds to the slope of $\ln(C(t))$.

responds to a backbone length of $L_z/10$. Since the charged groups of the monomers adopt a helix-like structure (see Fig. 4(a) in the main text) for the straightened PDADMA chain, we define the location of N$^+$ of the l^{th} monomer by $(r^l, \theta^l, z^l), l = 1,2,...,10$ in cylindrical coordinates with longitudinal axis parallel to (and centered at) the backbone of the PE. The ion number density around the l^{th} monomer (in the region $z^l - L_z/20 < z < z^l + L_z/20$) is projected into a two-dimensional density map $\rho^{\text{Cl},l}(r,\theta)$ in polar coordinates. The ion number densities around different monomers are similar but the angular orientation of the density follows the relative orientation of the monomer θ^l. To account for this, we rotate the ion number density map by $-\theta^l$ degrees as $\rho^{\text{Cl},l}(r,\theta-\theta^l)$, to overlay the orientations of the monomers such that superposed ion number density data in terms of orientation with respect to monomer is obtained. Then we take an average over $\rho^{\text{Cl},l}$ to get the density $\rho^{\text{Cl}} = \langle \rho^{\text{Cl},l}(r,\theta-\theta^l) \rangle_l$ for different salt concentrations as shown in Fig. S1(b). This ion number density distribution around the PE monomers concretely shows the origins of the two-peak profile in the ion distribution in the main manuscript: ions form a semi-circular ring around the charged group with ion condensation localization visible both at the sides and at the tip of the charged group, leading to the binodal ion number density distribution. Similar findings were already reported in Ref. 3. In particular, the Cl$^-$ ions stack mainly on the directions $\pm\pi/2$ and 0, corresponding to the first and the second peaks of Cl$^-$ in the radial density profiles, respectively. This configuration is caused by two main interactions on Cl$^-$ ions: attraction from positively charged group centered at N$^+$ atoms and steric repulsion from the surrounding neutral atoms. The positionally correlated configurations of the PE charge groups and its effect on the ion density span over different salt concentrations.

4 The orientational self-correlation function

The atomistic-detail PDADMA molecule spans the z axial direction of the simulation box as a periodic molecule. However, it can both translate and rotate along the z axis during the MD simulations. The orientation of the chain on the $z = 0$ plane is given by the angle θ^1 as defined in Fig. S1 ($l = 1$). During a 100 ns simulation we measured the time dependence of $\theta^1(t)$ and its time average $\bar{\theta}^1 = \langle \theta^1(t) \rangle_t$. We then define the normalized orientational (fluctuation) self-correlation function $C(t)$ as

$$C(t) = \frac{\langle \Delta\theta^1(s)\Delta\theta^1(s+t) \rangle_s}{\langle \Delta\theta^1(s)\Delta\theta^1(s) \rangle_s}, \tag{S4}$$

where $\Delta\theta^1 = \theta^1 - \bar{\theta}^1$. As an example, for a single PDADMA chain at salt concentration $\rho_0 = 0.26$ M, the self-correlation function decreases exponentially as $\exp(-t/t_c)$ as shown in Fig. S2. From this data we can estimate the self-rotational correlation time as $t_c \approx 15$ ns.

5 Comparison between SPB and SLPB theories

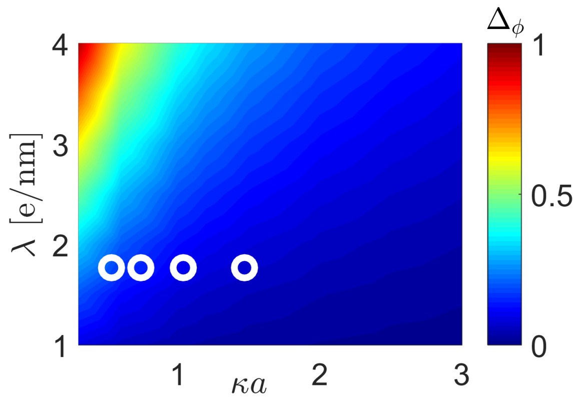

Fig. S3 The mean relative error of the electrostatic potential Δ_ϕ as a function of linear charge density λ and dimensionless effective radius κa. The circles represent the reference points for PDADMA with concentrations $\rho_0 =$ 0.13 M, 0.26 M, 0.52 M and 1.0 M, from left to right, respectively.

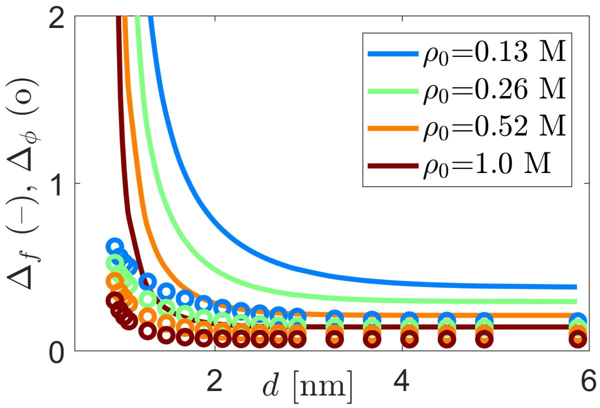

Fig. S4 The relative errors in the mean force Δ_f (lines) and electrostatic potential Δ_ϕ (circles) between the SPB and LSPB theories for the case of two PEs as a function of their separation.

We addressed the differences in the electrostatic potential $\phi_{\text{SPB}}(r)$ and $\phi_{\text{SLPB}}(r)$ with the same linear charge density λ, effective radii $a_{\text{SLPB}} = a_{\text{SPB}} = a$ and monovalent salt concentration ρ_0. A theoretical comparison between the two approximations is reported in Ref. 4. However, here we focus on PDADMA. The difference is expressed as the relative error $\Delta_\phi \equiv$

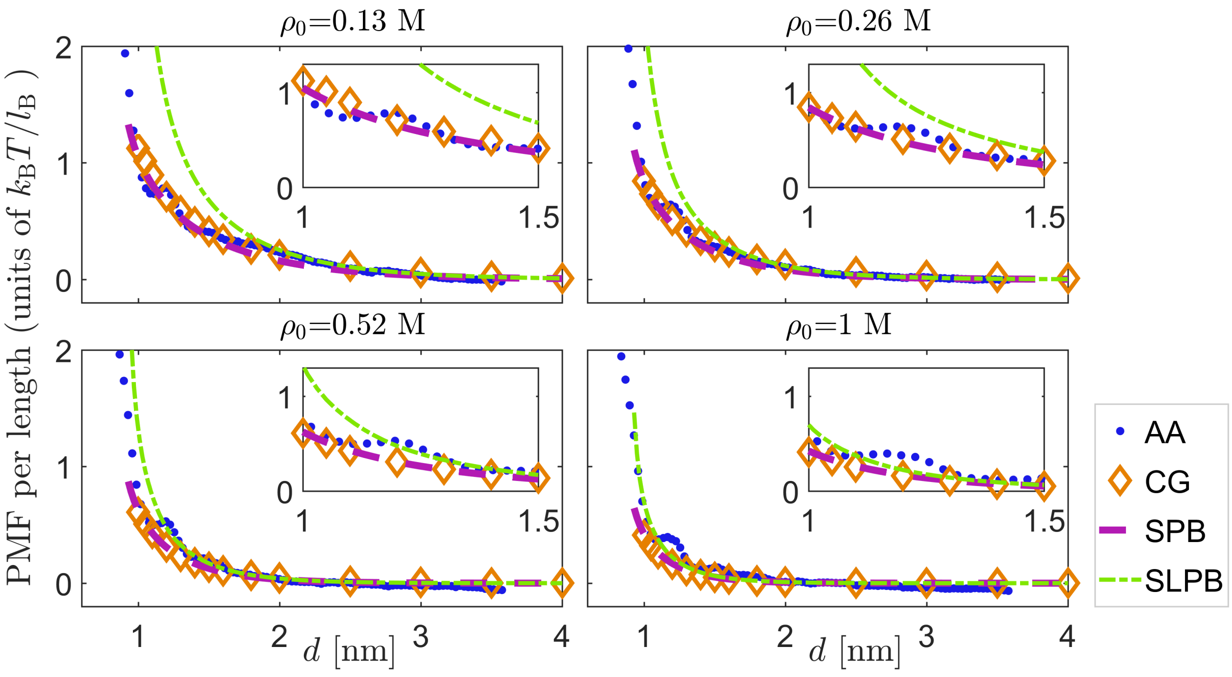

Fig. S5 Comparison between the PMFs as a function of distance d obtained from the different models and different salts. The abbreviation AA refers to all-atom MD simulations. The insets show details of the oscillating regions in the PMF profiles.

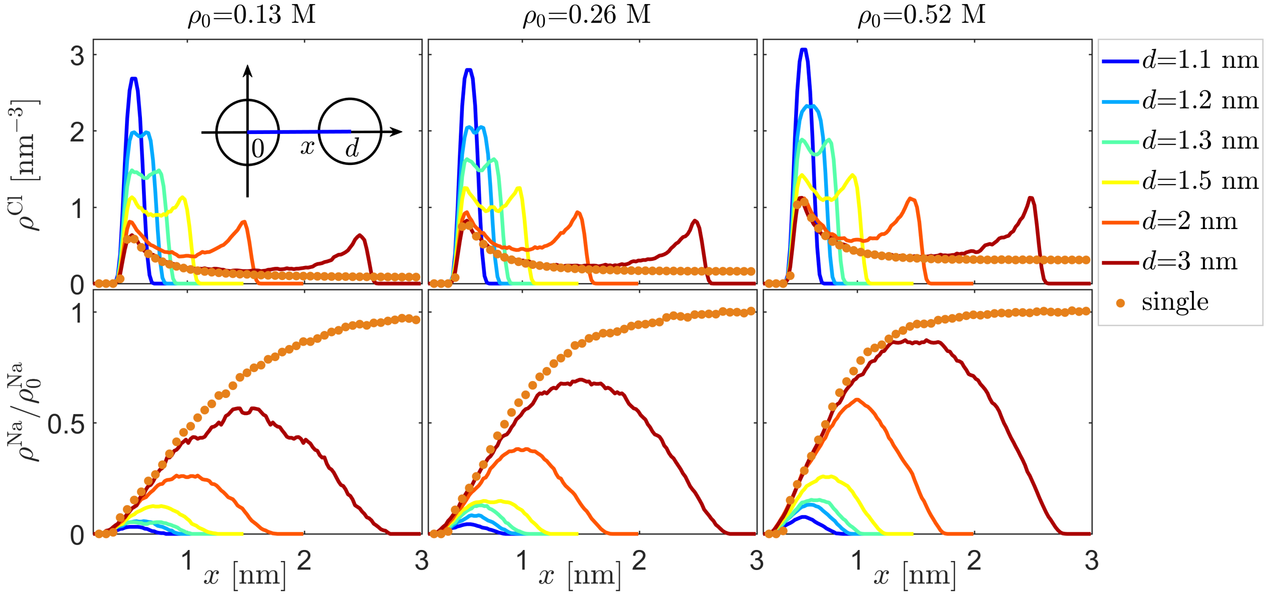

Fig. S6 The Cl$^-$ and Na$^+$ number density profiles along the x axis connecting the centers of the two PEs from the CG-MD model (as sketched in the inset). The center-to-center distance d changes from 1.1 nm to 3.0 nm.

$\langle|\phi_{\rm SLPB}(r)-\phi_{\rm SPB}(r)|/\phi_{\rm SPB}(r)\rangle_r$, which is averaged over $a<r<L_x/2$. Using the Debye length κ^{-1} as a unit of length, the only characteristic length scale in the system is κa. Thus, Δ_ϕ solely depends on λ and κa. We show this in Fig. S3. As expected, for large values of λ, small values of a and low salt concentration ρ_0 (corresponding to low κ), we find the highest-error region (red). We can see that in the case of PDADMA (circles), the PB and LPB are almost identical at all salt concentrations considered here. This is due to a relatively small linear charge density $\lambda = 1.767$ e/nm, giving rise to small electrostatic potential ϕ. We conclude that in the case of PDADMA the linear approximation is successful in capturing the ion distribution.

For the two-PDADMA case, the relative error of mean force and electrostatic potential at $x = d/2$ are expressed as $\Delta_f \equiv |f_{\rm SLPB}-f_{\rm SPB}|/f_{\rm SPB}$ and $\Delta_\phi \equiv \langle|\phi_{\rm SLPB}(d/2,y)-\phi_{\rm SPB}(d/2,y)|/\phi_{\rm SPB}(d/2,y)\rangle_y$, respectively; the latter is averaged over $-L_y/2<y<L_y/2$. Their comparison is shown in Fig. S4. In contrast to the single PE case, the mean

force from SLPB is very different from that of the SPB, especially when the two PEs are close.

6 Linear-linear scale figure of PMF

In Fig. 3 of the main manuscript we show a comparison between the PMFs between two identical PEs obtained from all-atom MD and CG-MD simulations, as well as from the SPB and SLPB theories. For completeness, in Fig. S5 we report the same data plotted on a linear-linear scale.

7 Ion density around two CG-MD PDADMAs

In the CG model, we can examine the ion number densities around two PEs. As shown in Fig. S7, a significant fraction of the Cl^- ions accumulate in the region between the two PEs when the distance between the two rods is relatively short ($d \leq 1.5$ nm). In Fig. S7 we report the two-dimensional number density for $d = 1.2$ nm and $d = 2.0$ nm.

To better quantify this, we obtained the one-dimensional cross section of the ion-number density profiles between the two PEs at $0 < x < d, y = 0$ (see the inset of Fig. S6) for different values of d, and compared them to the single-PE case, as shown in Fig. S6. When the two rods are close ($d = 1.1$ nm), the peak value of the Cl^- ion-number density is 3 to 4 times larger than that of the single-PE case. On the other hand, the Na^+ ion number density is much lower than that of a single rod. This is due to the stronger electrostatic repulsion, as well as the Cl^- ions occupying more space in between the rods.

8 Limitation of the SPB approach

In the original work of Vahid *et al.*[5] where the SPB theory was introduced it was applied to model monovalent ion distributions around single polystyrene sulphonate molecules. The corresponding ion densities were accurately reproduced for a wide range of system parameters, including salt and ion sizes. We performed additional testing for the case of two such PEs with atomistic-level MD simulations and the same setup as for the PDADMA molecules here. However, we found that there was an attractive force induced between two polystyrene sulphonate molecules at short distances. Such attraction is not expected in the weak-coupling regime and here it may be caused by entropy loss due to the axially straight, infinite PE chain simulation setup. Thus, we did not consider this case further in the present work.

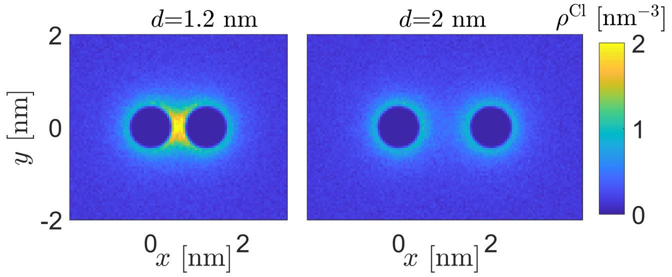

Fig. S7 The Cl^- density map around two rods with $d = 1.2$ nm and $d = 2.0$ nm from the CG-MD model. The added salt concentration is 0.26 M.

Notes and references

1 P. Grochowski and J. Trylska, *Biopolymers*, 2008, **89**, 93–113.
2 S. L. Brenner and V. A. Parsegian, *Biophys. J.*, 1974, **14**, 327–334.
3 P. Batys, S. Luukkonen and M. Sammalkorpi, *Phys. Chem. Chem. Phys.*, 2017, **19**, 24583–24593.
4 J. Philip and R. Wooding, *J. Chem. Phys.*, 1970, **52**, 953–959.
5 H. Vahid, A. Scacchi, X. Yang, T. Ala-Nissila and M. Sammalkorpi, *J. Chem. Phys.*, 2022, **156**, 214906.